#### Nyrkova L.

Doctor of Engineering Sciences Senior Researcher E.O. Paton Electric Welding Institute of the National Academy of Sciences of Ukraine Department of gas and oil pipes welding Ukraine

#### Goncharenko L.

Researcher
E.O. Paton Electric Welding Institute of the
National Academy of Sciences of Ukraine
Department of gas and oil pipes welding
Ukraine

#### Osadchuk S.

Candidate of Engineering Sciences Senior Researcher E.O. Paton Electric Welding Institute of the National Academy of Sciences of Ukraine Department of gas and oil pipes welding

#### Kharchenko Yu.

Post graduate student E.O. Paton Electric Welding Institute of the National Academy of Sciences of Ukraine Department of gas and oil pipes welding Ukraine

# Analyzing the Effect of Long-term Operation of Gas Pipeline of X70 Steel on Stress-corrosion Cracking Susceptibility in Near-neutral pH Solution Under Cathodic Polarization

Stress-corrosion cracking of the parent metal of linear section of main gas pipeline of X70 steel after operation for 40 years in near-neutral pH solution NS4 was investigated in comparison with the pipe that was not in operation and sheet steel. The tensile strength and yield strength all studied specimens meet the requirements of ISO 3183, but the relative elongation the specimens from pipes is slightly below the normalized value. Corrosion potentials are similar and equal to -0.697 V for sheet steel, -0.681 V for new pipe, -0.689 for exploited pipe, and the corrosion rates are 0.053, 0.064 and 0.056 mm/year, respectively, which corresponds to the resistance group "stable". Stress-corrosion cracking at potentials negatively than the maximum protective -1.050 V occurs by the hydrogen mechanism for a new pipe, and for the sheet and pipe after 40 years of operation - by mechanism of anodic dissolution and hydrogen embrittlement with a small contribution of anodic dissolution. At the potential of -1.050 V, hydrogen penetration is greatest for the sheet steel (0.045  $mol/dm^3$ ), for the new pipe and pipe after 40 years of operation – values are similar, 0.0296 and 0.0241 mol/dm<sup>3</sup>, respectively.

**Keywords:** X70 steel, pipeline, long-term operation, corrosion, stress-corrosion cracking, hydrogen penetration.

#### 1. INTRODUCTION

In the modern world, the main type of natural gas transportation is pipeline transport; therefore, its safety and reliability have an important impact on the economic development of different countries and security [1,2]. Underground gas mains during operation under conditions of complex anti-corrosion protection (protective coatings and electrochemical induction of cathodic polarization) are subject to the joint influence of mechanical and corrosion factors. When designing, the properties of object are selected so that during construction and during long-term operation, even under adverse conditions, the object was capable of maintaining the specified indicators at the required level and withstanding external factors during operation.

In several studies devoted to assessing the condition of pipeline transporting gas after long-term exploitation, deterioration of the condition of the pipe metal has been reported. One of the main factors, which is leading to steels degradation, deformation aging is noted, as a result of which strength increases and plasticity and impact toughness decrease [3]. According to some indicators of the mechanical properties, metals from such sections of pipeline steel do not meet the requirements of regulatory documents [4]. The pipes properties of

Received: April 2025, Accepted: August 2025 Correspondence to: Dr Ludmila Nyrkova, E.O. Paton Electric Welding Institute of the National Academy of Sciences of Ukraine, K. Malevich Str. 11, Kyiv, Ukraine E-mail: lnyrkova@gmail.com

doi: 10.5937/fme2504607N

various production technologies (hot-rolled and controlled rolling) do not change equally, which is probably due to the influence of metallurgical factors. Thus, for steel 13GS, the aging process is accompanied by an increase in the yield area during rupture without a noticeable effect on strength; for X70,  $\sigma_y$  and, accordingly,  $\sigma_{st}/\sigma_y$  increases [4-6]. In addition, the effect of aging was accompanied by an increase in the critical brittleness temperature to -20 °C.

Some researchers consider the development of volumetric microdamage to be the reason for this [7,8], which, in our opinion, is more characteristic of pipelines transporting hydrogenated media and less characteristic of gas pipelines. There are data [9] on the shift of the corrosion potential of operated steels to more negative values and an increase in the corrosion current; however, the reason for this phenomenon is not sufficiently understood.

The presence of surface microdelamination after the rupture of specimens of operated steels is controversial. Some authors argue that the viscous appearance of cracks with splits is characteristic of X70 steel, which is manufactured using controlled rolling technology in the temperatures (20 – -80) °C [10]. Other authors view the surface micro-stratification of fractured specimens from used pipes as diffuse damage to the metal, resulting from the structure and absorbed hydrogen [11].

According to the results of studies on pipes of different grades, it was found that the parent metal and welded joints retain high operational properties after long-term operation 12]. Due to the high viscosity and plasticity of the initial metal, its condition after pro—

longed operation can be considered satisfactory [13]. It is anticipated that the most significant changes in the physical and mechanical properties of controlled-rolled X70 steels, resulting from operational influences, will occur in localized areas where defects, stress concentrators, deformed zones, and similar factors are present [14,15].

In soil environment under cathodic protection and mechanical stresses in cites of protective polymer coating detachment, one of the most dangerous types of destruction is stress-corrosion cracking [16,17].

Stress corrosion cracking can occur in solutions with high pH in concentrated carbonate-bicarbonate solutions (pH>9.0) [18-20] and in solutions with pH close to neutral (at pH  $\sim$  6.5) [21-24].

As follows from the analysis of literature sources, the results of research devoted stress-corrosion cracking of metals in long-term gas pipelines are insufficient.

In our previous papers [22,26] the influence of different factors and their combinations on the sensitivity of X70 steel to SCC were investigated. The methodical approach for estimating SCC based on the simulation of different combinations of stress-corrosion factors and the evaluation of their effect on the sen–sitivity of pipe steel to SCC according to the criterion  $K_s$  was developed. Scientific merit of this paper is in the expansion of theoretical ideas regarding stress-corrosion cracking of long-exploited steel X70 under cathodic polarization in a model soil electrolyte NS4.

The aim of this work is to investigate the influence of the long-term operation of metal pipes of main gas pipelines made of X70 steel on their susceptibility to stress-corrosion cracking under conditions of cathodic polarization in near-neutral environment.

#### 2. MATERIAL AND METHODS

#### 2.1 Materials

Investigations were conducted in model soil electrolyte NS4 with the composition, g/l: 0.122 KCl + 0.483 NaHCO<sub>3</sub> + 0.181 CaCl<sub>2</sub> + 0.131 MgSO<sub>4</sub> [25]. Distilled water and chemical pure reagents were used for its preparation. Specimens were weighed on laboratory-analytical scale VLR-200 g.

This study was conducted using the following specimens:

- low-alloy ferritic-pearlite steel of X70 grade (sheet)
- base metal of a pipe that was not in operation (hereinafter referred to as a new pipe);
  - base metal of pipe after 40 years of operation. Specimens were cut perpendicular to the rolled stock.

#### 2.2 Electrochemical tests

The specimens were ground on abrasive paper with different grain sizes, then with magnesium oxide, washed and dried. The potential and polarization curves were measured using a pressure cell. The corrosion potentials of the studied steels were measured for 30 min. Anodic and cathodic polarization curves were recorded at a potential scanning rate of 1<sup>-3</sup> V/s using potentiodynamic regime. The universal device potenti—

ostat–galvanostat MTech PGP-550F with MTech PGP-550F software and control via a USB interface was used. The permissible reduction in error of the setting/measuring voltage/current was 0.15%.

X70 steel, saturated silver chloride electrode (SSCE), and platinum electrode were used as working, reference and auxiliary electrodes.

Polarization curves of slow and fast scanning of potential were recorded at a rate of 0.5 and 100 mV/s from -1.2 V to 0.5 V.

#### 2.3 Massometry method

The corrosion rate was determined by massometry on three specimens. After degreasing, the specimens were kept in the MLW 117-0200 chamber at a temperature of plus (105-110) °C to a constant mass, weighed, and their area was determined using an electronic caliper. The specimens were kept in solution for 168 h (one week). At the end of the tests, the specimens were washed with running tap water, the corrosion products were removed using an eraser, rinsed, and dried at a temperature of plus (105-110) °C to a constant mass, and weighed. The corrosion rate in g/(m²·h) was calculated based on the change in the specimen mass and duration of the studies.

#### 2.4 Slow strain rate tests

For studies using the slow strain rate tests, the specimens were manufactured according to a sketch (Fig. 1).

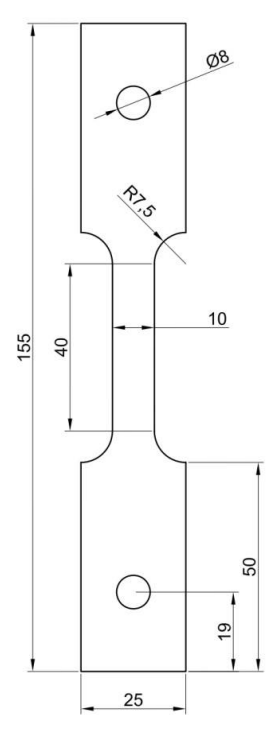


Figure 1. Specimen's drawing for slow strain rate tests

An AIMA-5-1 tensile machine, the specimens deformation rate was 10<sup>-6</sup> s<sup>-1</sup>, the conditions of periodic wetting with a solution (50 min in the solution and 10 min in air), and the applying of cathodic polarization at potentials of -0.750 V, -0.950 V, -1.050 V and -1.200 V was used [13]. The reference and auxiliary electrodes were the same as those used in the electrochemical experiments. Photo of

electrochemical cell for SCC research under cathodic polarization is presented in Figure 2.



Figure 2. Photo of electrochemical cell for SCC research.

Susceptibility to SCC was estimated by the formula (1). For quantifying the SCC sensitivity of X70 steel the dimensionless coefficient  $K_S$  [26] was used:

$$K_{S} = \frac{\psi_{air}}{\psi_{sol}} = \frac{\left(S_{0} - S_{1}^{air}\right) / S_{0}}{\left(S_{0} - S_{1}^{sol}\right) / S_{0}} \tag{1}$$

where  $\psi_{air}$  relative narrowing of specimens in air;

 $\psi_{sol}$  relative narrowing of specimens in the solution;

 $S_0$  is the cross-section area of specimens before tests, mm<sup>2</sup>;

 $S_1^{air}$  is the cross-section area of specimens in the place of fracture after tests in air, mm<sup>2</sup>;

 $S_1^{sol}$  is the cross-section area of specimens in the place of fracture after tests in the solution, mm<sup>2</sup>.

#### 2.5 Metallographic and fracture investigations

Specimens for metallographic analysis were made using diamond pastes of different dispersion. To reveal the microstructure 4% nitric acid in ethyl alcohol was used. Metallographic studies were performed on a microscope NEOPHOT 21 with digital camera Allied Vision 1800 U-2050c and software SEO ImageLAB.

Specimens surface after breaking were investigated y SEM method on a JSM 840 microscope. Secondary backscattered electron mod, accelerating voltage 20 kV, and  $(10^{-7}-10^{-10})$  A electron beam current were used.

#### 2.6 Hydrogen penetration tests

Electrolytic penetration study of hydrogen into X70 steel was performed as in our previous works were described [24]. The research was carried out at polarization potentials -0.750 V, -0.950 V, -1.050 V. Concentration of hydrogen, which penetrating through steel specimens was determined as it presented in ISO 17081 [27]:

$$C_H = \frac{I_{st} \cdot L}{D_H \cdot FS} \tag{2}$$

 $I_{st}$  – current at stationary hydrogen penetration regime, A;

S – specimen's square, m<sup>2</sup> (0.00096 m<sup>2</sup>);

F – Faraday constant, 96485 C/mole;

 $D_{H_2}$  – hydrogen diffusion coefficient,  $1.5 \cdot 10^{-9}$  cm<sup>2</sup>/c;

 $C_{H_2}$  – concentration of hydrogen penetrating into the metal, mole/m<sup>3</sup>;

L – specimen thickness, m.

$$I_{st} = I_{H_2} - I_b \tag{3}$$

 $I_{H_{\bullet}}$  – current caused by hydrogen penetration, A;

 $I_b$  – background current equal to the current of specimen passivation, A.

Effective coefficient of hydrogen diffusion was calculated for fulfilling the condition  $J(t)/J_{st}=0.63$  [23, 27]:

$$D_{H_2}^{ef} = \frac{L^2}{6\tau_{0.63}} \tag{4}$$

 $\tau$  – time duration, min.

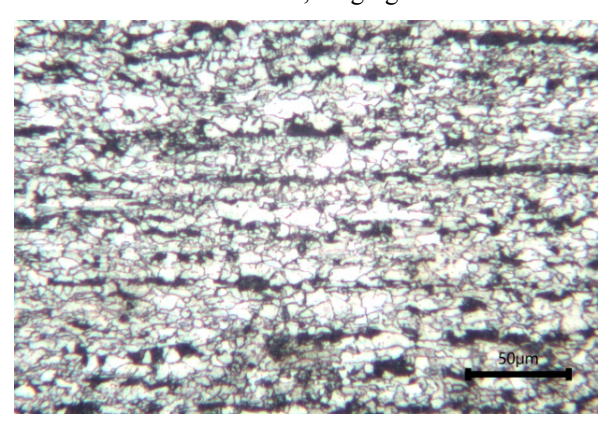
#### 3. RESULTS AND DISCUSSION

#### 3.1 Microstructure

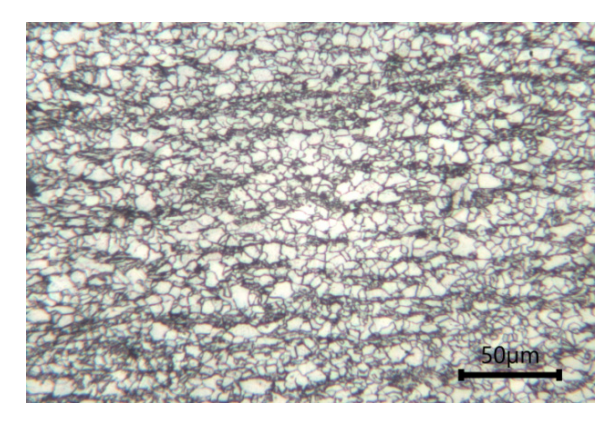
Microstructure of the sheet steel specimens is ferrite and pearlite mixture of (Fig. 3, a).

The average diameter of the ferrite grain is from 0.011-0.006 mm according to [28]. Pearlite components were located mainly along the ferrite grains boundaries, and the pearlite component amount was near (10-12) %. Ferrite grains are deformed, which indicates on controlled rolling manufacture of steel. Small carbide particles were observed in ferrite grains. The striation of the base metal is developed and is equal to 4-5 points in series B according to the State Standard of Ukraine 8974 [29].

The microstructure of the specimens of X70 steel, made from new pipe, consisted of small ferrite grains and bainite formations (Fig. 2, b). The size of the ferrite grains was mostly in the range of 0.006–0.015 mm. The bainite grains are also small, with a diameter of approximately 0.005 mm, and are arranged in a discontinuous strip along the rolling of the metal. The volume of bainite formation is small, ranging from 5 to 7%.



а



b

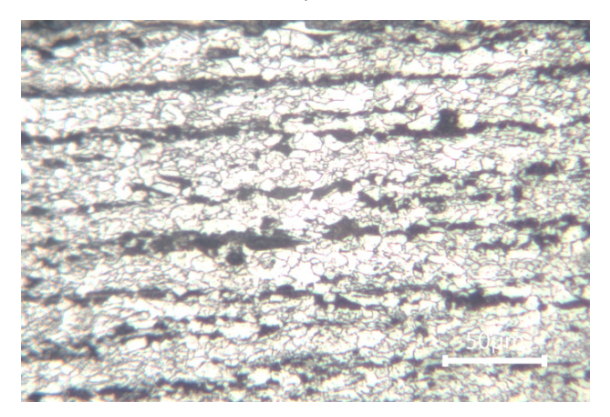


Figure 3. Microstructure : a – sheet; b – new pipe; c – pipe after 40 years of operation

Microstructure of operated pipe (during 40 years) metal is also typical for controlled rolling steel and consists of ferrite and pearlite mixture (Fig. 2, c). Ferrite grains were mostly deformed, and the size of the ferrite grains ranged from 0.006 to 0.018 mm. The stripes of the pearlite component are continuous and correspond to four points in Series B [29]. The volume of the pearlite component is approximately 17% larger than that of the metal in the other pipes. Carbide particles were discovered in ferrite grains bodies.

#### 3.2 Chemical composition

Table 1. Chemical composition of investigated specimens

Chemical compositions of the specimens is presented in Table 1.

From analysis of content of the main alloying elements, it can be stated that the metals of the sheet, new pipe, and pipe after 40 years of operation meet the requirements of both ISO 3183 [30] and TR 14-3-995 [31] (Table 1). It should be noted that the Mn content in the new pipe and exploited pipe was closer to the value specified in ISO 3183.

In terms of tensile strength and yield strength, specimens made from sheet, new pipe and used pipe meet the requirements of TR 14-3-995 (Table 2). The elongation was slightly lower than the normalized value.

#### 3.3 Corrosion and electrochemical properties

To determine the impact of the operational factors that underground gas pipelines are exposed to during operation, in particular, the effects of prolonged mechanical loads, corrosive environments, and cathodic polarization, massometric studies were conducted, and the corrosion rate of X70 steel in different states was determined. The following specimens were studied — made of sheet, new pipe and pipe after 40 years of operation.

The appearance of the surface after testing is shown in Fig. 4. After the corrosion tests, the surface of the sheet steel specimens was covered with a thin layer of dark brown corrosion products (Fig. 4, a); specimens from a new pipe, and an operated pipe —with a layer of light brown corrosion products (Fig. 4, b, c).

The determined constant values of corrosion potentials in the NS4 solution are equal for specimens: from a sheet -0.697 V, a new pipe -0.681 V, and a pipe after 40 years of operation -0.689 V (Fig. 5, a, b), that is, they are somewhat more positive. The corresponding anodic slopes were 0.063, 0.038, and 0.036 V curves (Fig. 5, c).

The values of the corrosion rate of steel are close, 0.053, 0.064, and 0.056 mm/year, which, according to the corrosion resistance scale, characterizes steel in the NS4 solution as "resistant" (Table 3).

Specimen characterization,	C	Mn	Si	S	P	Al	Mo	V	Nb
RD requirements									
X70 (sheet)	0.096	1.71	0.208	0,009	0.007	0,035	0.03	0.06	0.052
New pipe	0.075	1.43	-	-	-	-	< 0.03	0.02	0.027
Pipe after 40 years of	0.09	1.39	0.40	0,006	0.023	0,021	< 0.01	0.071	0.029
operation									
TR 14-3-995[31]	0.12	1.70	0.50	0,010	0.020	0,050	0.30	0.08	0.06
Requirements of ISO 3183[30]	0.280	1.40	-	-	-	-	Nb+N	10+V not more t	han 0,15

Table 2. Mechanical properties of investigated specimens

Characterization of specimen, regulatory document	σ <sub>ts</sub> , MPa	σ <sub>y</sub> , MPa	δ, %
Sheet steel X70	485	570	20,0
New pipe	512,3	596	17,6
Pipe after 40 years of operation	491,4	588,2	18,7
TR 14-3-995	441	588	20

Table 3. Electrochemical properties of X70 steel in different states in NS4 solution

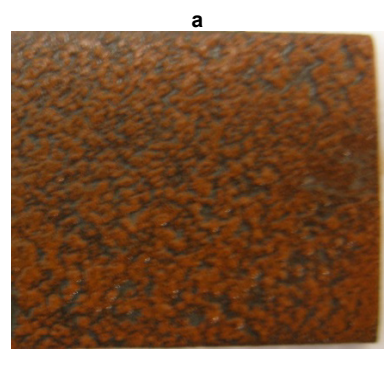
Specimen characterization	$E_{cor}$ , V	$b_a$ , V	$E_0^{-1}$ , V	$E_0^2$ , V	Mixed mechanism range, V	<i>v<sub>cor</sub></i> , mm/year
X70 (sheet)	-0.697	0.063	-1.001	-1.085	0.084	0.053
New pipe	-0.681	0.038	-0.682	-1.050	0.368	0.064
Pipe after 40 years of operation	-0.689	0.036	-0.920	-1.080	0.160	0.056

#### 3.4 Fast and Slow Potential Scan rate Curves

Sow and fast potential scanning curves of specimens of X70 steel in different states in the NS4 solution are shown in Fig. 6. To determine the limits of the ranges of changes in the stress-corrosion cracking mechanism, a theoretical model was used, which is discussed in detail by Parkins [16].

The potentials at zero current for a sheet specimen are -1.001 V and -1.085 V (Fig. 6, a). Therefore, in the NS4 solution at potentials range positively -1.001 V, SCC occurs according to anodic dissolution mechanism, at potentials negatively -1.085 V – according to hydrogen embrittlement mechanism. In potentials range from -1.001 to -1.085 V, SCC occurs according to anodic dissolution and hydrogen embrittlement mechanism simultaneously.





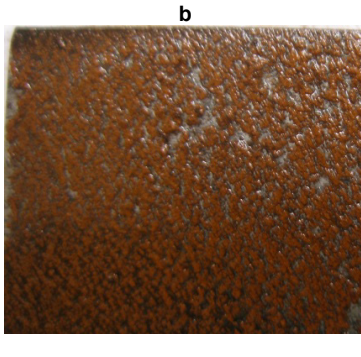
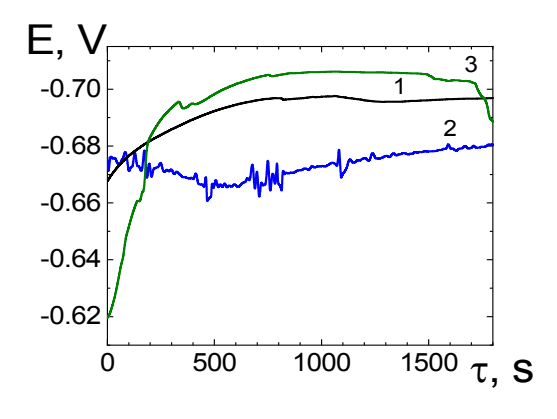
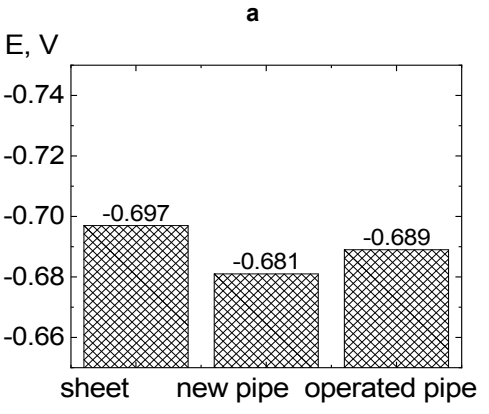


Figure 4. Appearance of the specimens after testing for 168 hours at room temperature in NS4 solution: 1 – sheet; 2 – new pipe; 4 – pipe after 40 years of operation





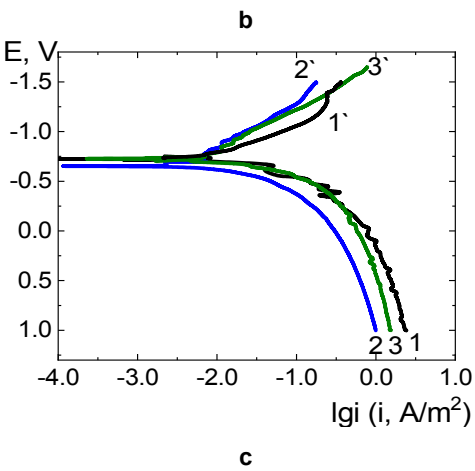
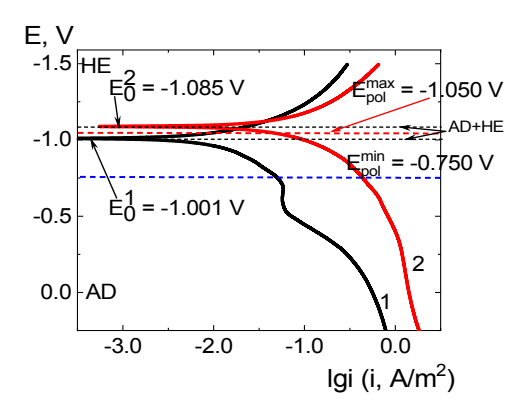
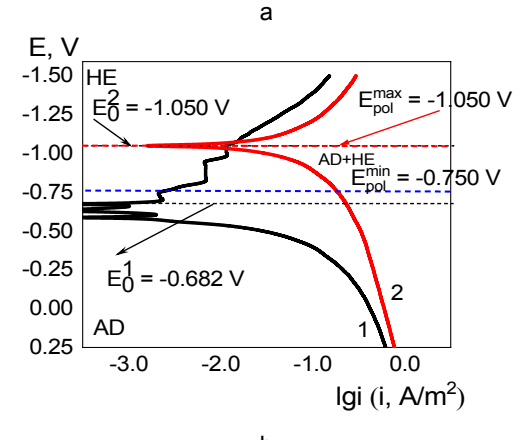


Figure 5. Appearance of the surface of the specimens after testing for 168 hours at room temperature in NS4 solution: 1 – sheet; 2 – new pipe; 4 – pipe after 40 years of operation

For the new pipe, the following limits for the stress-corrosion cracking potentials ranges were established: from -0.682 V and -1.050 (Fig. 6, b). That is, at potentials positively -0.682 V, anodic dissolution mechanism of SCC prevailed, and at potentials negatively -1.050 V, it occurs according to the hydrogen embrit-tlement mechanism. In the range of potentials from -0.682 V to -1.050 V, SCC occurs according to anodic dissolution and hydrogen embrittlement mechanisms.





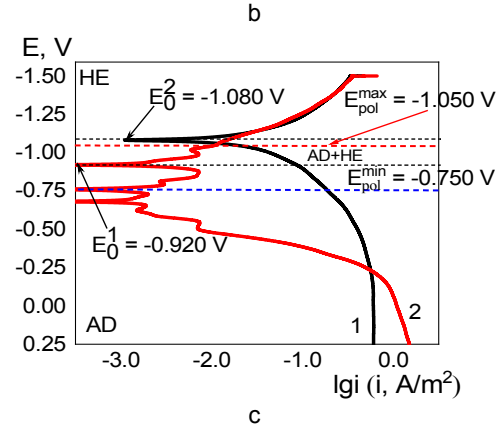


Figure 6. Potentiodynamic polarization curves in NS4 solution of steel X70 in different states: a – sheet; b – new pipe; c – pipe after 40 years of operation. Potential scanning rate: 1 – 0.5 mV/s; 2 – 100 mV/s

For a pipe after 40 years of operation, the lower and upper limits of the potential ranges were determined to be from -0.920 V to -1.080 (Fig. 6, c). Similarly, at potentials positively than -0.920 V, SCC occurs by anodic dissolution mechanism; at potentials from -0.920 V to -1.080 V, both mechanisms – anodic dissolution and hydrogen embrittlement took place; and at more negative

potentials than -1.080 V, exclusively hydrogen embrit-tlement mechanism is being imple-mented.

Thus, it was established that SCC of steel at potentials more negative than the maximum protective potential of -1.050 V occurs by the hydrogen embrittlement mechanism for a new pipe, but for the sheet and pipe after 40 years of operation at this potential, stress-corrosion cracking is still possible by the mixed mechanism with a small contribution of anodic dissolution. At potentials more positive than the minimum protective potential of -0.750 V, stress-corrosion cracking according to the anodic dissolution mechanism occurs only for the steel sheet and pipe after 40 years of operation, but for a new pipe at the minimum protective potential, stress-corrosion cracking is possible by the mixed mechanism.

Some narrowing of the range of action of the mixed mechanism for the pipe after 40 years of operation compared to the new pipe, 0.368 and 0.160 V in the NS4 solution is noted. It is assumed that the differences are due to both changes in the metal during pipe manufacturing on the one hand, and the influence of operational factors on the other side.

#### 3.5 Slow strain rate tests

The fracture diagrams of the specimens are shown in Fig. 7.

#### 3.5.1 Sheet specimens

The destruction of the sheet specimen in the air is accompanied by its narrowing near the breaking area, resulting in the formation of plastic deformation areas (Fig. 8, photo 1a). Breaking time was 43 h, relative elongation and narrowing was, respectively 74.95% 28.0% (Table 4).

At minimum protective potential of -0.750 V in NS4 solution, the breaking also occure predominantly viscously, and the rupture line was wavy but more complex than in the air (Fig. 8, photo 2a). The destruction time was 44 h, relative elongation was 28.5%, and narrowing decreased to 72.57% (Table 4). The coefficient of susceptibility to stress-corrosion cracking  $K_S$ , was 1.03.

The rupture of the specimen during the tests at a potential of -0.950 V on a larger surface area proceeded viscously (Fig. 8, photo 3a). A decrease in the fracture time to 41 h and relative narrowing to 68.80% were observed, but the relative elongation increased slightly to 29.0% (Table 4). The  $K_S$  coefficient increases to 1.09.

Table 4. Indicators of X70 steel in different states after slow strain rate tests in air and in NS4 solution at different polarization potentials

Experimental conditions, potential, V	$\tau_{break},h$	δ, %	S, mm <sup>2</sup>	ψ, %	$K_s$	Character of fracture morphology
				Sheet		
Air	43	28.00	7.51	74.95	-	Viscous
- 0.750	44.0	28.5	8.23	72.57	1.03	Viscous
-0.950	41.0	29.0	9.36	68.80	1.09	Viscous with brittle fragments
-1.050	39.0	25.6	10.40	65.31	1.15	Viscous with brittle fragments
- 1.200	39.0	24.8	13.91	53.6	1.40	Mostly brittle

			N	ew pipe		
Air	37.0	23.5	7.9	73.67	-	Viscous
- 0.750	37.5	22.7	8.31	72.31	1.02	Viscous
-0.950	38.1	21.4	10.05	66.50	1.10	Viscous with brittle fragments
-1.050	44.0	26.4	7.73	74.24	1.00	Viscous with brittle fragments
-1.200	34.5	20.5	7.57	74.78	1.00	Viscous with brittle fragments
		Pi	ipe after 40	years of ope	eration	
Air	33	19.1	8.79	70.71	-	Viscous
- 0.750	30	17.1	13.09	56.37	1.25	Viscous
-0.950	27	15.71	14.30	52.57	1.34	Viscous with brittle fragments
-1.050	30	14.8	16.16	46.12	1.53	Viscous with brittle fragments
- 1.200	30	15.71	18.60	37.99	1.86	Mostly brittle

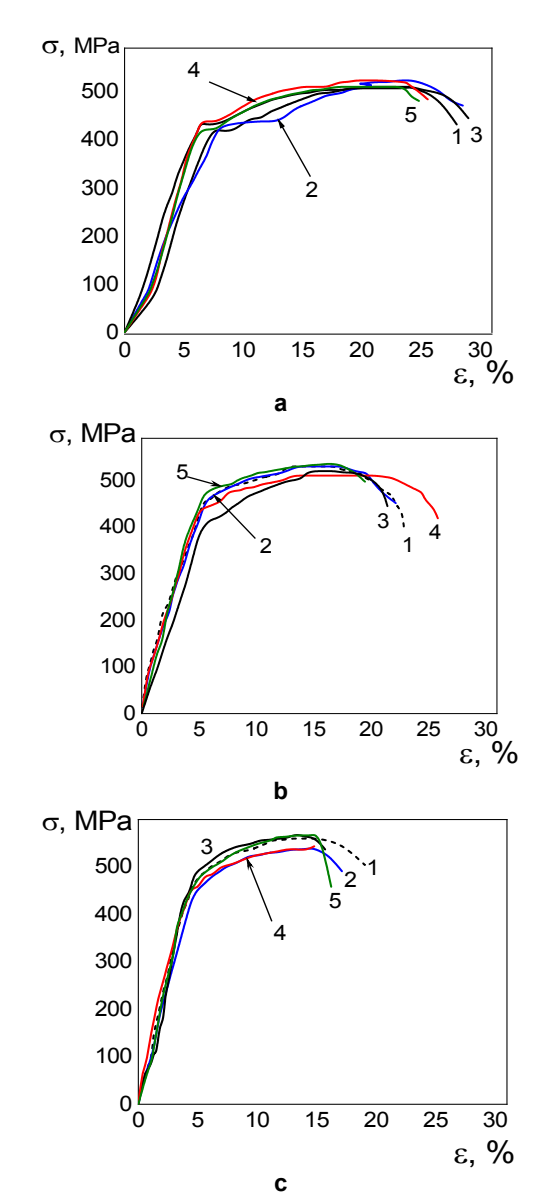


Figure 7. Fracture diagrams of X70 steel specimens after slow strain tests in air (1), and in NS4 solution at polarization potentials: 1 - 0.750 V; 2 - 0.950 V; 4 - 1.050 V; 5 - 1.200 V. 4 - 2.00 V

At the maximum protective potential of -1.050 V, the brittle fracture prevailed, the narrowing of the specimen was noticeably less, the fracture line was step-shaped and broken, and secondary cracks were visible (Fig. 8, photo 4a). The fracture time of the specimens continued to decrease to 39 h, relative elongation to 25.6%, and relative narrowing to 65.31% (Table 5),  $K_S$  increased to 1.15.

At a potential negatively than maximum protective potential, -1.200 V, relative elongation decreased to 24.8%, relative narrowing – to 53.6%, and an increase in  $K_S$  to 1.40 were noted. The fracture line was complex and broken, and secondary cracks were visible (Fig. 8, photo 5a).

#### 3.5.2 New pipe specimens

The destruction of specimens from a new pipe in air is also accompanied by the narrowing of the specimen near the rupture site, as a result of which areas of plastic deformation are formed (Fig. 8, photo 1b). The fracture time was 37 hours, relative elongation – 23.50%, relative narrowing – 73.67% (Table 4).

At a minimum protective potential of -0.750 V, the breaking also developed predominantly viscously, the rupture line was wavy, but more complex than in air (Fig. 8, photo 2b). The fracture time was 37.5 hours, the relative elongation decreased to 22.7%, the relative narrowing increased to 72.31% (Table 4),  $K_S$  is equal to 1.02.

Tests at polarization of -0.950 V in the NS4 showed that the fracture of the specimen over a larger surface area proceeds predominantly viscously, the fracture line is wavy (Fig. 8, photo 3b). At this potential, decrease in the fracture time of the specimens to 38.1 hours was observed, relative elongation decreased to 21.4%, relative narrowing was 66.5% (Table 4). The coefficient  $K_S$  increased to 1.10.

At maximum protective potential of -1.050 V, both brittle and ductile fragments in the fracture, the specimen narrowing is noticeably less, Table 4, there are step-like sections on the rupture line, the line is rather broken (Fig. 8, photo 4b). But the fracture time of the specimens even increased to 44 hours, relative elongation to 26.4%, relative narrowing increased to 74.24% (Table 5), and  $K_{\rm S}$  was equal to 1.00.

At potential of -1.200 V, the greatest decrease in the fracture time to 34.5 hours, decrease in relative elongation to 20.5%, and increase relative narrowing to 74.78% were observed (Fig. 8, photo 5b).  $K_S$  did not change and was equal to 1.00.

#### 3.5.3 Exploited pipe specimens

The breaking of specimens from the pipe after 40 years of operation in the air, as for the previously considered specimens, was accompanied by the formation of a plastic deformation area near the rupture line, (Fig. 8, photo 1c). The breaking time was 33 h, relative elongation was 19.1%, and relative narrowing was 70.71% (Table 4).

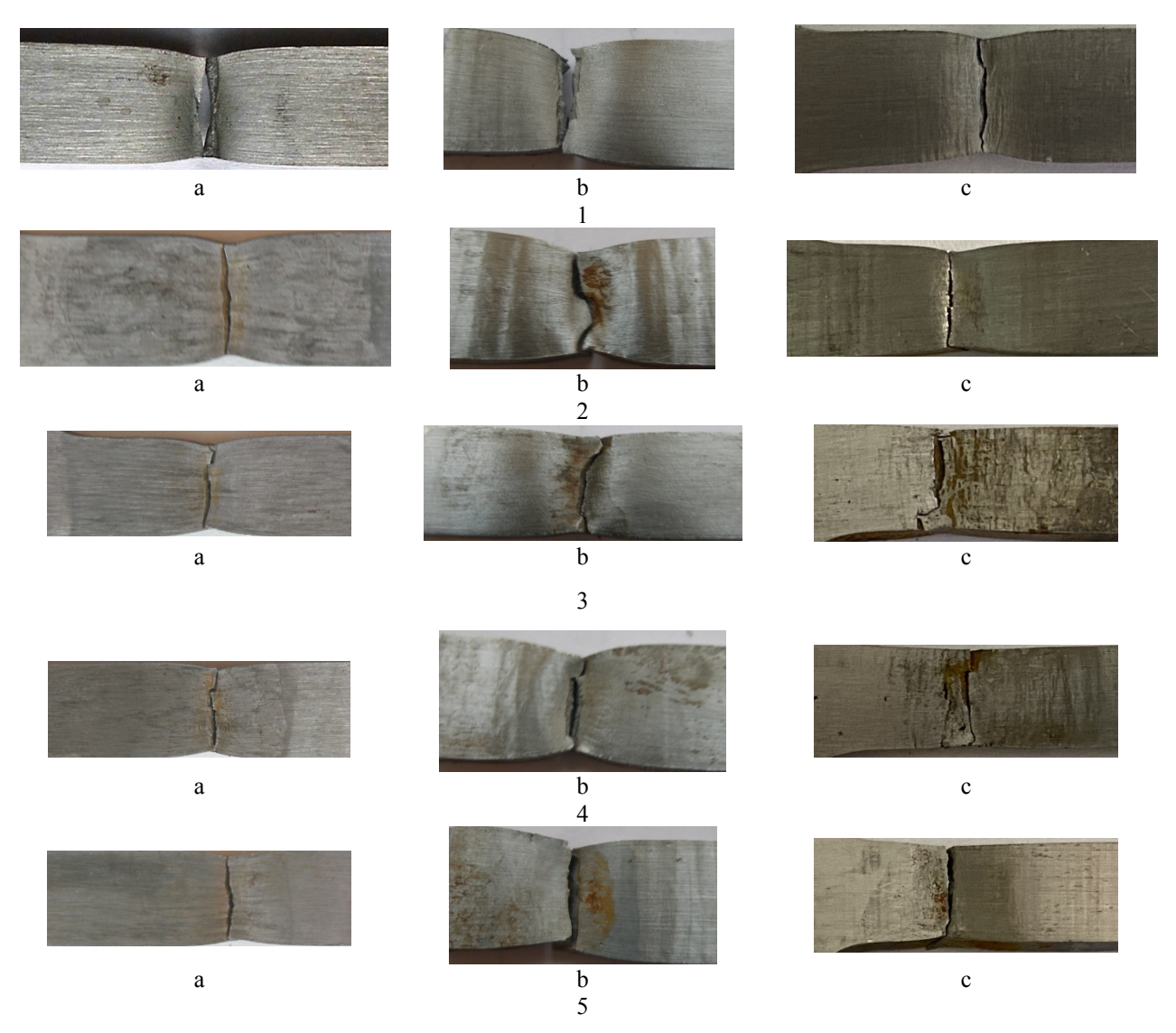


Figure 8. Appearance of the rupture area of specimens of X70 steel after slow strain rate tests in air (1), and in NS4 solution (2-5) at polarization potentials: 2 - 0.750 V; 3 - 0.950 V; 4 - 1.050 V; 5 - 1.200 V; a - sheet; b - new pipe; c - pipe after 40 years of operation

At a minimum protective potential of -0.750 V, destruction developed mainly viscously (Fig. 8, photo 2c,). The destruction time decreased to 30 hours, relative elongation – to 17.1%, the relative narrowing to – 56.37% (Table 5),  $K_S$  was 1.25.

At a potential of -0.950 V, a change in the appearance of the rupture line is observed, which takes the form of a complex broken line (Fig. 8, photo 3c). At this polarization potential, a decrease in the fracture time of the samples to 27 h and a relative elongation of 15.71% were observed, whereas the relative narrowing was 52.57% (Table 5). The  $K_S$  coefficient increases to 1.34.

At a maximum protective potential of -1.050 V, brittle nature prevails in the fracture, and a decrease in the plastic deformation of the sample is visually noted (Fig. 7, photo 4 c), and the rupture line is step-shaped broken. The failure time was 30 h, relative elongation decreased to 14.8%, and relative narrowing – to 46.12% (Table 5), which caused a natural increase in  $K_S$  to 1.53.

At potential -1.200 V, there is also a noticeable decrease in the plastic deformation of the specimen (Fig. 8, photo 5c); the fracture line is step-shaped with small steps, and the fracture time is the same as at

-1.050 V, that is, 30 h, the relative elongation was 15.71%, the relative narrowing decreased to 37.99%, and  $K_{\rm S}$  increased to 1.86. Analyzing the features of corrosion-mechanical fracture of specimens in the potential range from -0.750 V to -1.20 V, the following should be noted.

It is inappropriate to compare steel in different states with each other, since it is not from the same batch (because it is difficult to ensure the performance of comparative tests over a long period of time), may differ the manufacturing technology used at the manufacturing plant, and has differences in chemical composition. The most rationally assess how much the corrosion-mechanical properties of steel change under corrosive environment influence of a compared to air and draw conclusions; based on such considerations, it will be possible to note the degree of influence of the operating environment on a possible change in properties. It is usually advisable to consider the entire complex of metal properties, in particular chemical composition, microstructure, strength and ductility indicators, corrosion, electrochemical, susceptibility to hydrogenation, and corrosion-mechanical properties.

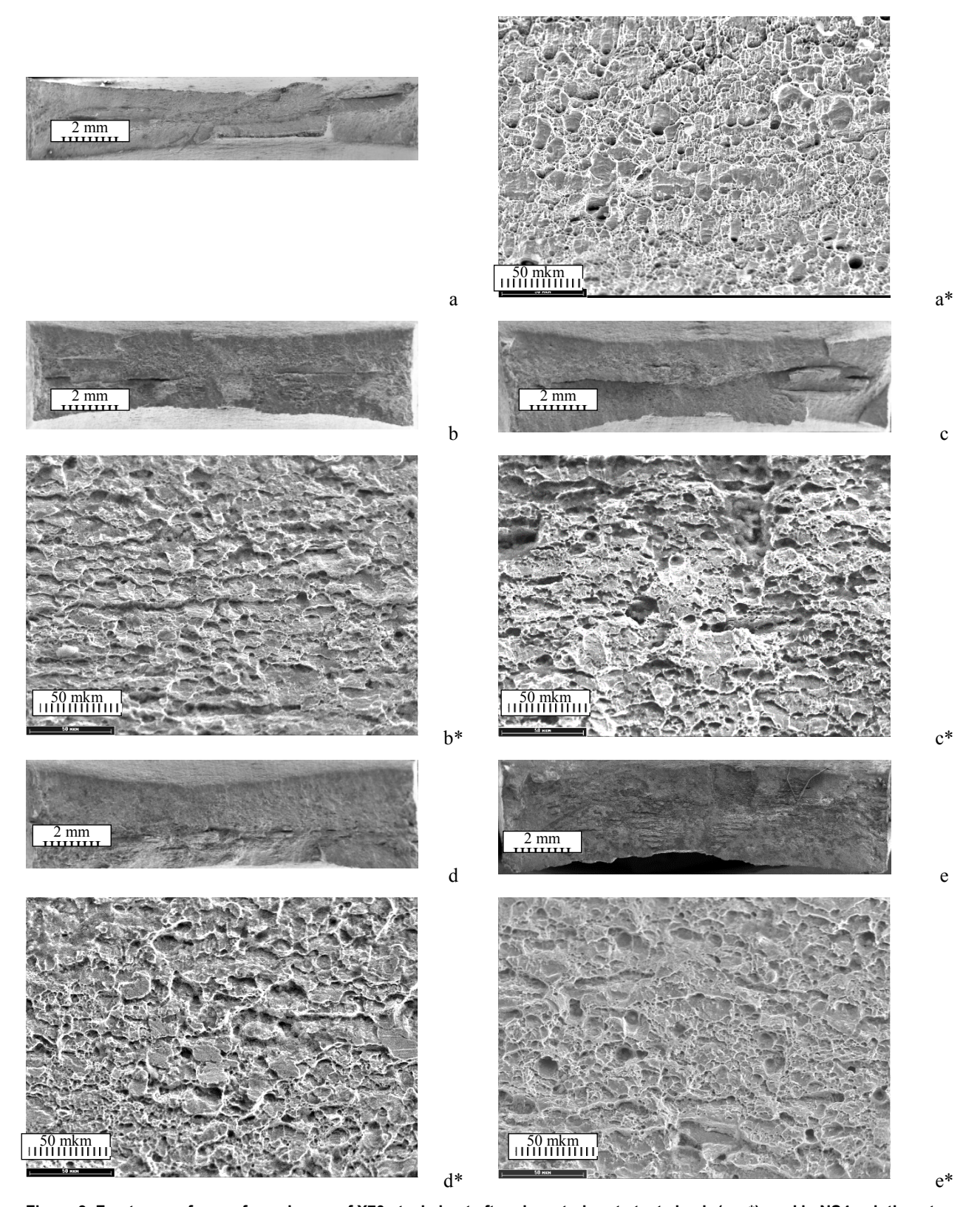


Figure 9. Fracture surfaces of specimens of X70 steel sheet after slow strain rate tests in air (a,  $a^*$ ), and in NS4 solution at polarization potentials: b,  $b^*$  -0.750 V; c,  $c^*$  --0.950 V; d,  $d^*$  --1.050 V; e,  $e^*$ --1.200 V

So, it was found that when the cathodic polarization potential is shifted in the range -0.750 V  $\rightarrow$  -0.950 V  $\rightarrow$  -1.050 V  $\rightarrow$  -1.200 V, the susceptibility to stress-corrosion cracking in the solution, which is estimated by the coefficient  $K_S$ , changes for a steel sheet as  $1.03 \rightarrow 1.09 \rightarrow 1.15 \rightarrow 1.40$ ; for a new pipe in the range  $1.02 \rightarrow 1.10 \rightarrow 1.00 \rightarrow 1.00$ ; for a pipe after 40 years of operation such as -1.25  $\rightarrow$  1.34  $\rightarrow$  1.53  $\rightarrow$  1.86.

### 3.6 Investigation of the fracture of specimens after slow strain rate tests

#### 3.6.1 Sheet specimens

The fracture surface after breaking in air has pronounced signs of plastic deformation, which is evident in the pits formed during the destruction of non-metallic inclusions (Fig. 9, a, a\*). Along with the areas of ductile

pitting fracture caused by detachment, there are fragments of ductile shear fracture elements. The size of the pits corresponded to the size of the grains. Pearlite stripes appeared on the fracture surface, while the larger flat pits resulted from the shear fracture of pearlite colonies (with a grain size of approximately 22  $\mu m$ ) due to plastic deformation.

The fractographic details of the relief after rupture of the samples in solution at -0.750 V indicate the viscous pitting nature of the fracture. As a result of the shear and detachment fractures, larger pits were formed (Fig. 9, b, b\*). In pore fusion zones, shear facets are formed under the action of deformation. A section of the initial cleavage stage was detected.

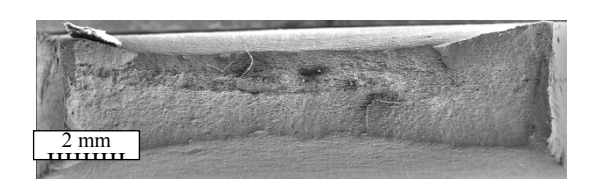
The fracture surface of the specimen at a potential of -0.950 V exhibited more heterogeneous nature than that of air (Fig. 9, c, c\*). There are pits of different diameters: small and shallow, with lower energy consumption compared to air, and deep pits with nonmetallic inclusions at the bottom. There are also many cleavage facets up to 20 µm in size, which were formed due to separation of combined small pores with undeveloped viscous bridges, as well as during the separation of pearlite grains arranged in the form of stripes. Small cleavages were detected, which are characteristic of controlled-rolling steel. The presence of several local loose zones is noted without signs of plastic deformation, which can be assumed to be a consequence of hydrogen damage to the metal.

At a maximum protective potential of -1.050 V (Fig. 9, d, d\*). The fracture pattern of the specimen was mixed along with small pits with a carbide phase at the bottom. Elements of brittle fracture were found: facets of intergranular fracture cleavage with a diameter of approximately 30  $\mu$ m, as well as deep pits with a diameter of approximately 20  $\mu$ m. The proportion of pitted ductile fractures was much smaller than that of brittle fractures.

A small part of the fracture surface at -1.200 V in NS4 contained crimp cleavage (Fig. 9, e, e\*). Pits of various sizes were observed, formed by the union of smaller pits with larger ones, in particular, planes of viscous shear.

Thus, the type of fracture under these conditions can be attributed to a mixed ductile-brittle nature. The frac-

2 mm



a

ture pattern was significantly different from that observed at the minimum protective potential -0.750 V.

#### 3.6.2 New pipe specimens

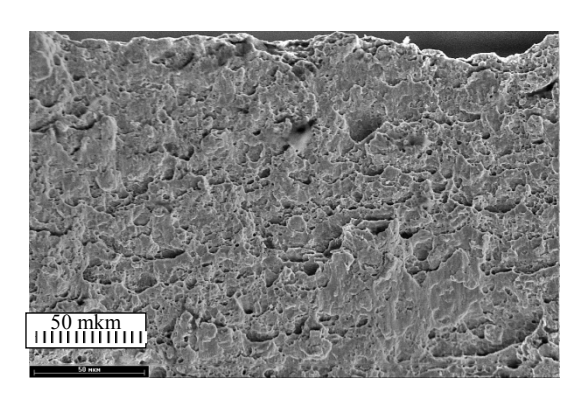
The fracture surface of a specimen from a new pipe after testing in air demonstrated ductile fracture with a relatively homogeneous nature. The fractographic structure of the fracture surface indicates that it occurred through the rupture of small pits and plastic shear deformation. Apart from individual small crack-like discontinuities that are in the initial stage of cleavage development, there are no signs of striation (Fig. 10, a, a\*).

After slow strain rate tests at -0.750 V, the fracture of the specimens according to the fracture characteristics was also viscous (Fig. 10, b, b\*). It can be noted that the fracture structure is almost similar to the fracture of the specimens tested in air, its nature corresponds to shear deformation.

At -0.950 V, the fracture is mainly viscous, but with a lower fracture energy (Fig. 10, c, c\*). The surface appearance differs from the fractures formed under the first two test conditions by larger fracture details in the form of pits up to 25  $\mu m$  in size formed by the union of small pores and extended quasi-brittle fragments. The bottom of the pits was not smooth and reflected the metal structure. Destruction occurred under the shear deformation component.

When tested at a potential of -1.050 V, the nature of the fracture was viscous, and the fracture appearance was smoothed owing to shear deformation. It is possible to note a slightly noticeable increase in crack-like longitudinal discontinuity delaminations, which occur in controlled rolling steels with a decrease in fracture energy (Fig. 10, d, d\*).

After slow strain rate tests at a potential of -1.200 V, the fracture also occurred according to the viscous characteristics (Fig. 10, e, e\*). The destroyed part of the specimen near the surface corresponds to plastic shear deformation, and the other part is due to shear deformation and rupture. It is possible to note the formation of extended small parabolic-shaped elongated cavitiespits with diameters of up to 20  $\mu m$  with small inclusions at the bottom.



a\*



c

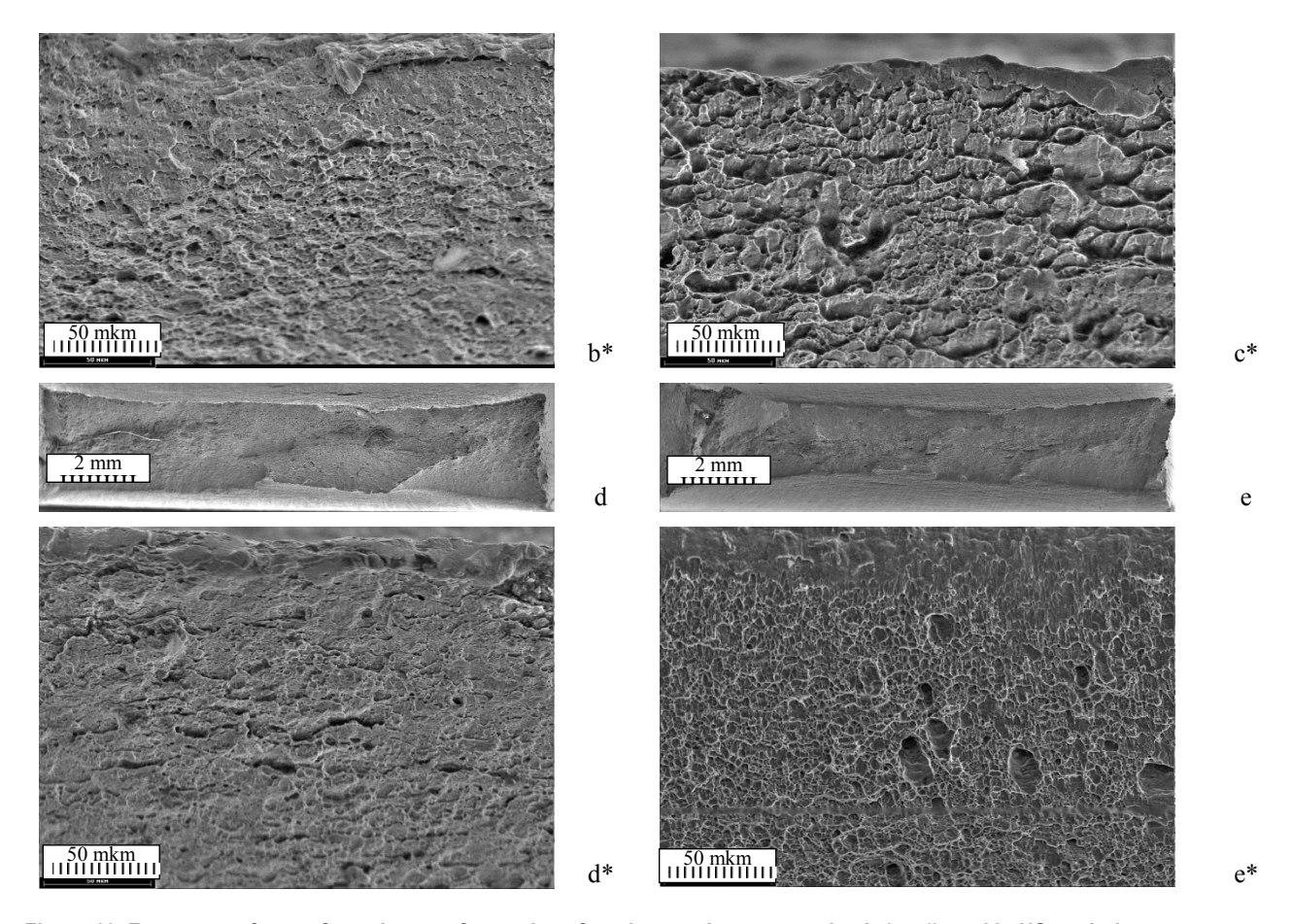
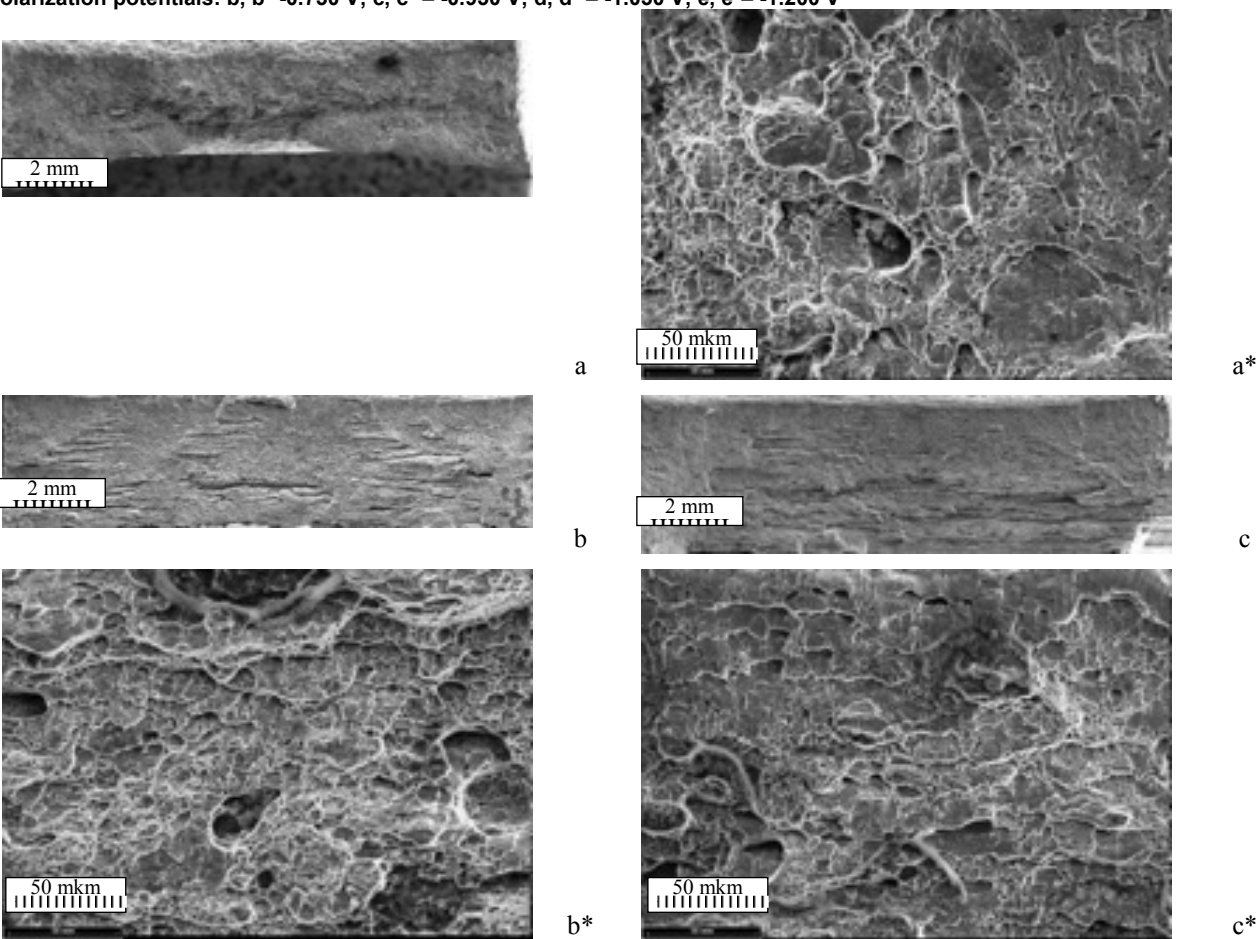


Figure 10. Fracture surfaces of specimens of new pipe after slow strain rate tests in air (a, a\*), and in NS4 solution at polarization potentials: b, b\* -0.750 V; c, c\* - -0.950 V; d, d\* - -1.050 V; e, e\*- -1.200 V



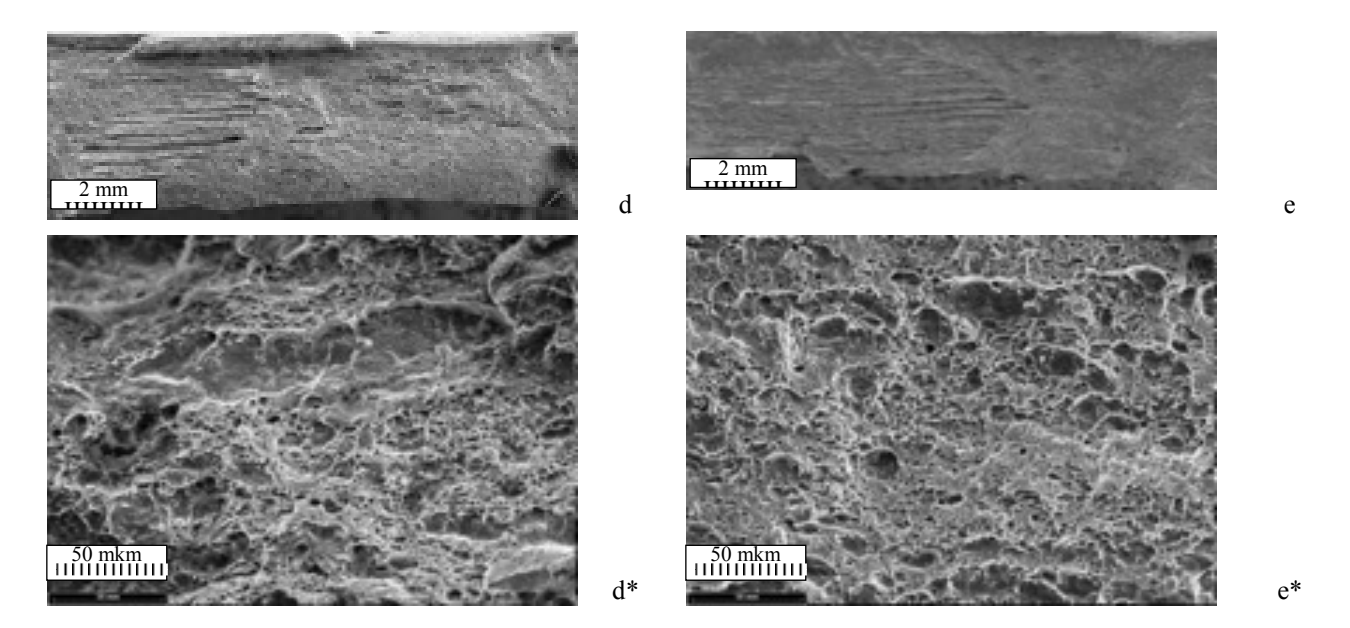


Figure 11. Fracture surfaces of specimens of pipe after 40 years of operation after slow strain rate tests in air (a, a\*), and in NS4 solution at polarization potentials: b, b\* -0.750 V; c, c\* -0.950 V; d, d\* -0.750 V; e, e\*-0.750 V; e,

#### 3.6.3 Exploited pipe specimens

The fracture surface of the pipe specimen after 40 years of operation after tests in air had a heterogeneous structure (Fig. 11, a, a\*). The fracture details are mostly of a viscous nature and are formed according to the mechanism of nucleation, growth, and merging of micro holes. Most of the pits were small, with other single large pits with diameter of (40-60) microns. The fracture ridges are developed but not over the entire plane, which confirms the inhomogeneity in terms of the strength of the detachment of the ductile nature of the fracture. There are several smoothed fragments with an almost flat bottom and barely noticeable small details, which can be attributed to low-energy quasi-brittle fracture along the grain boundaries. Several deep pits with non-metallic inclusions were observed.

After slow strain rate tests at -0.750 V, the fracture structure was almost the same as that of the specimen tested in air (Fig. 11, b, b\*). However, there is a difference in that the fracture consists of pits of smaller size and depth, with lower energy intensity. The elongation of the pores and the presence of detachment ridges due to plastic deformation were noted. Damage to the metal in the form of shallow flat cavities due to intergranular fracture was noticeable.

After testing at -0.950 V, destruction occurred through the mechanism of joint deformation (Fig 11, c, c\*). The fracture surface is composed of flat, shallow, and large fragments that were formed after the merger of smaller pits with weak grain boundaries. The fracture surface was characterized by weakly developed deformation ridges. The formation of quasi-critical facets was also recorded.

After slow strain rate tests at a potential of -1.050 V, the breaking surface exhibited a heterogeneous rough structure (Fig. 11, d, d\*). The plots with fragmentary pits were located in a row with quasi-crystal fragments and a zone with ripple-like structures. A long, very large empty hole of up to 150  $\mu m$  may indicate the local weakening of the metal.

After slow strain rate tests at a potential of -1,200 V, the surface of the ruin also exhibited a rough heterogeneous structure (Fig. 11, e, e\*). Breaking surface consists of small pores, dotted with empty pits of different configurations and larger facets of a friable appearance (the largest size is 20 microns), which are grouped in stripe zones and most likely agree the development of pearlite bands.

## 3.7 Investigation of the influence of the metal condition on the susceptibility to electrolytic hydrogenation in NS4 solution under cathodic polarization

Fig. 12-14 presents the experimental results of the hydrogenation study of X70 steel in different states. The passivation potential in the oxidation chamber was set at -0.250 V.

As can be seen from the results presented in Fig. 12, for specimens of X70 steel made of sheet, in the oxidation chamber at cathodic polarization at -0.750 V and at -0.950 V in NS4 solution, no increase in current due to hydrogen penetration was observed, and the value of the background currents during the entire measurement time only decreased. At maximum protective potential of -1.050 V, two current jumps of 0.0079 mA and 0.0160 mA were observed. These current values correspond to hydrogen concentrations of 0.057 and 0.114 mole/m³ for a potential of -1.050 V (Table 5). At potential -1.200 V, an increase in the current of 0.0025 mA was observed relative to the background value, which corresponds to calculated concentration of hydrogen 0.018 mole/dm³ (Table 5). The delay in hydrogen reduction was 25 min.

As can be seen from the results presented in Fig. 13, for a new pipe made of X70 steel in the NS4 solution at cathodic polarization potentials from -0.950 V to -1.200 V in oxidation chamber, an increase in current, which corresponded to the penetration of hydrogen, was observed.

In the potentials range -0.950 V  $\rightarrow$  -1.050 V  $\rightarrow$  -1.200 V, the hydrogen permeation current changed as

follows 0.0025 mA  $\rightarrow$  0.0037 mA  $\rightarrow$  0.0036 mA (Table 5), which corresponded to concentration of hydrogen of 0.0175 mole/m³  $\rightarrow$  0.0296 mole/m³  $\rightarrow$  0.0301 mole/dm³ (Table 5). As can be seen from the data in Fig. 14, on specimens of X70 steel, made from a pipe after 40 years of operation, in the range of cathodic polarization potentials from -0.850 V to -1.200 V, an increase in the current in the oxidation chamber due to hydrogen penetration was observed.

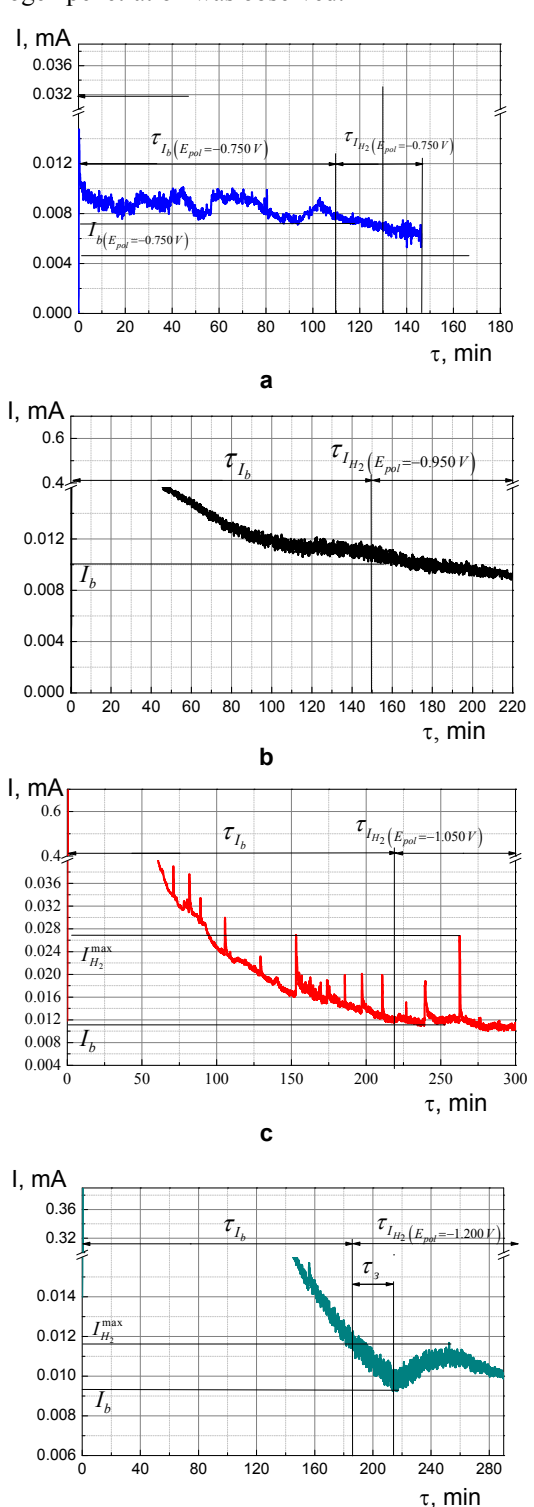


Figure 12. Change in current on X70 steel sheet specimens in an oxidation chamber in NS4 solution at polarization potentials: a – -0.750 V; b – -0.950 V; c – -1.050 V; d – -1.200 V

d

When the potentials were shifted in the series -0.850 V  $\rightarrow$  -0.950 V  $\rightarrow$  -1.050 V  $\rightarrow$  -1.200 V, the hydrogen permeation current changed as follows: 0.00083 mA  $\rightarrow$  0.0025 mA  $\rightarrow$  0.0032 mA  $\rightarrow$  0.0058 mA (Table 2.31), which corresponded to hyd-rogen concentration of 0.0062 mole/m³  $\rightarrow$  0.0191 mole /m³  $\rightarrow$  0.0241 mole/m³  $\rightarrow$  0.0397 mole/m³ (Table 5). The hydrogen delay time was set, respectively, 32 min  $\rightarrow$  25 min  $\rightarrow$  6 min  $\rightarrow$  12 min.

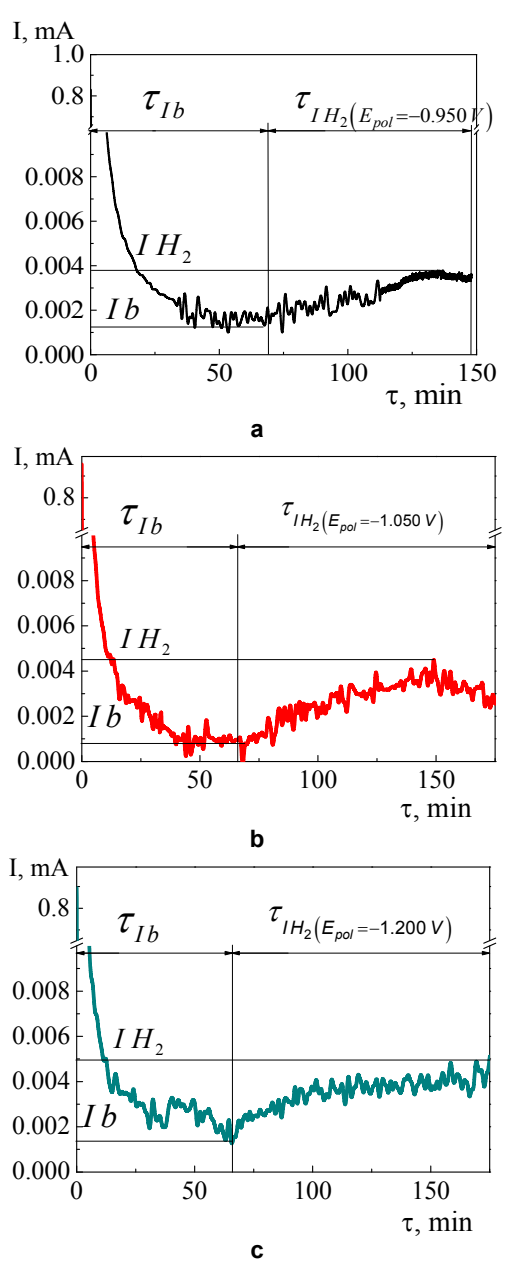


Figure 13. Change in current on X70 steel specimens of a new pipe in an oxidation chamber in NS4 solution at polarization potentials: a - -0.950 V; b - -1.050 V; c - -1.200 V

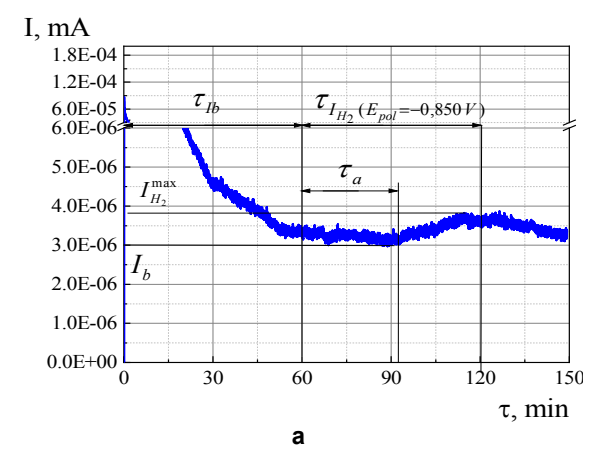
It was found that dependence of the concentration of hydrogen penetrating into steel under cathodic polarization is nonlinear, Fig. 15.

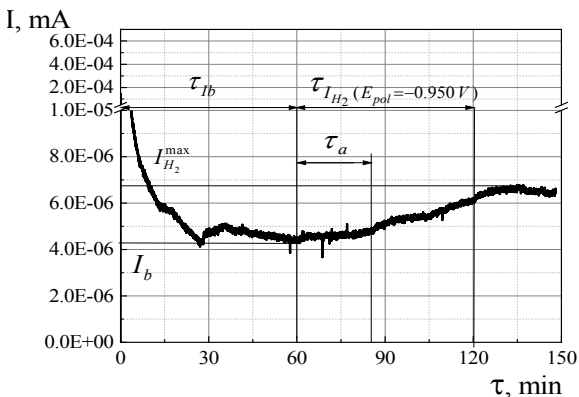
Following features of hydrogen penetration were noted for the studied specimens [23, 24]:

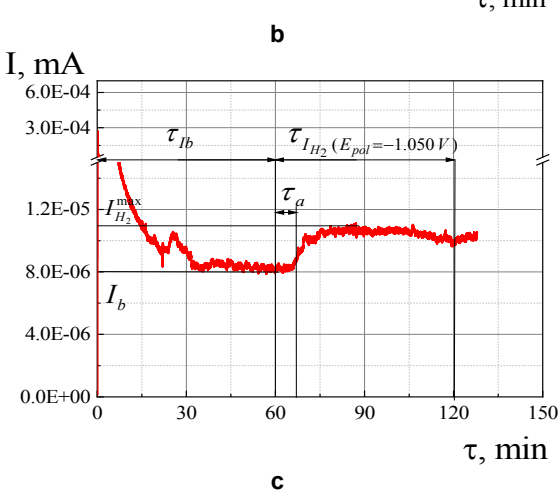
- for the sheet of steel specimens, maximum hydrogenation at a potential of -1.050 V (0.045 mole /dm³), when potential shifted to -1.20 V – hydrogen concentration decreased to 0.018 mole/dm³.

Table 5. Electrochemical characteristics of the hydrogenation of X70 steel specimens at different cathodic polarization potentials

$E_{pol}$ , V	$E_{cor}$ , V	$I_b$ , mA	$I_{H_2}$ , mA	I <sub>st</sub> , mA	L, m	C <sub>0</sub> , mole/dm <sup>3</sup>		
	Sheet							
-0.75	-0.695	0.0073	-	-	0.001	-		
-0.95	-0.762	0.0100	-	-	0.00099	-		
-1.05	-0.864	0.0109	0.0188	0.0079	0.001	0.057		
-1.20	-0.838	0.0092	0.0117	0.0025	0.001	0.018		
	New pipe							
-0.95	-0.745	0.00125	0.00379	0.0025	0.00096	0.0175		
-1.05	-0.764	0.0008	0.00448	0.0037	0.00112	0.0296		
-1.20	-0.789	0.00132	0.00493	0.0036	0.00116	0.0301		
		Pipe a	fter 40 years of ope	eration				
-0.85	-0.738	0.00297	0.0038	0,00083	0.00104	0.0062		
-0,95	-0.722	0.0042	0.0067	0.0025	0.00106	0.0191		
-1,05	-0.708	0.0079	0.01108	0.0032	0.00106	0.0241		
-1.20	-0,706	0.0056	0.01144	0.0058	0.00088	0.0397		







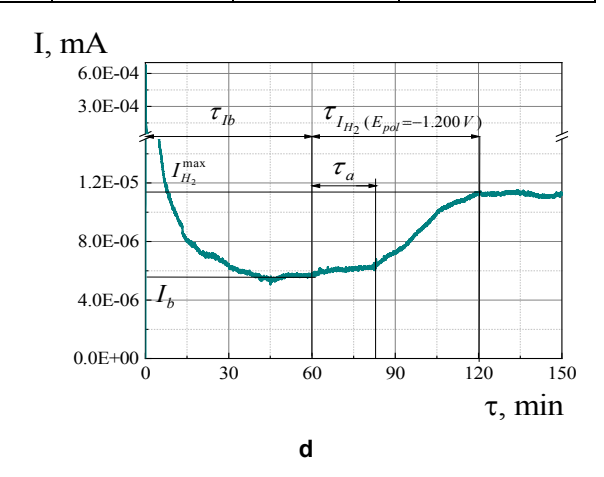


Figure 14. Change in current on X70 steel specimens made from a pipe after 40 years operation in an oxidation chamber in NS4 solution at polarization potentials: a - 0.750 V; b - 0.950 V; c - -1.050 V; d - -1.200 V

- for a new pipe and a pipe after 40 years of operation – an increase in hydrogenation when a potential shifted from -0.950 to -1.200 V; for a new pipe, an increase in the amount of hydrogen from 0.0175 to 0.0296 mole/dm³ when potential shifted from -0.950 V to -1.050 V and a slowdown near the value of 0.0301 mole/dm³ at a potential of -1.200 V is characteristic. For specimens from the pipe after 40 years of operation, the amount of hydrogen gradually increases from 0.0191  $\rightarrow$  0.0241  $\rightarrow$  0.0397 mole/dm³ with a potential shift of -0.950 V  $\rightarrow$  -1.050 V  $\rightarrow$  -1.200 V.

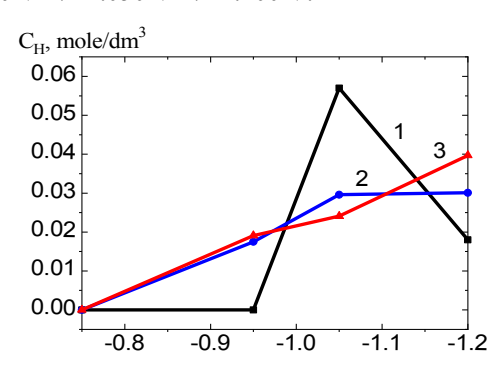


Figure 15. Concentration of hydrogen penetrating through steel at cathodic polarization: 1 – sheet of X70 steel; 2 – new pipe; 3 – pipe after 40 years of operation

Summarizing the above experimental results, scientific novelty of the work was formulated – theoretical conception regarding stress-corrosion cracking of long-term exploited X70 steel under cathodic polarization in a model soil electrolyte NS4 was expanded, which consists in determining the SCC mechanism and susceptibility to SCC in the normalized range of protective potentials from -0.750 V to -1.050 V [32]. A narrowing of the width of the mixed range of corrosion cracking potentials for long-serviced metal was revealed: from 0.368 V for a new pipe to 0.160 V for an operated pipe. The coefficients of susceptibility to SCC Ks which proposed in previous paper [26] at a potential of -1.05 V increase for steel after long-term operation and are, respectively, 1.10, and 1.53.

Also practical applications of the work was estab-

- the susceptibility to electrolytic hydrogenation in NS4 of X70 steel after operation for 40 years in the range of protective potentials regulated by National Standard 4219 [32] does not deteriorate compared to the susceptibility to hydrogenation of the new pipe metal.
- for a main gas pipeline after 40 years of operation, SCC by the hydrogen embrittlement mechanism, which is the most dangerous, begins at potentials more negative than -1.080 V, which is lower than the absolute value of the maximum protective -1.050 V.

Further safe operation of main gas pipelines is possible under conditions of strict compliance with the requirements of the standards for the level of cathodic protection.

#### 3. CONCLUSION

The following conclusions were drawn from the results of the research.

- 1. The microstructure of specimens of X70 steel, has the following characteristic features:
- sheet ferrite and pearlite mixture, the average diameter of ferrite grains is from 0.011-0.006 mm, pearlite particles are disposed along the ferrite grains boundaries, pearlite component amount is (10-12) %, ferrite grains are deformed, there are small carbide formations on the grain body, striation is 4-5 points, series B;
- new pipe a mixture of small ferrite grains and bainite formations, the size of ferrite grains is from 0.006 to 0.015 mm, bainite grains approximately 0.005 mm, their volume is from 5 to 7%;
- operated pipe (40 years) mixtures of ferrite and pearlite with deformed ferrite grains, ferrite grain size from 0.006 to 0.018 mm, stripes of pearlite component are continuous and correspond to 4 points, series B, volume of pearlite component is 17%, small carbide particles were found in ferrite grains.
- 2. According to the content of main alloying elements, the metal of the sheet, new pipe and pipe after 40 years of operation meets the requirements of both DSTU ISO 3183 and TR 14-3-995. The manganese content in the metal of a new pipe and a pipe after 40

years of operation is closer to the standard DSTU ISO 3183.

- 3. In terms of tensile strength and yield strength, samples made from sheet, new and operated pipes meet the requirements of TR 14-3-995, the relative elongation is slightly below the standard value.
- 4. Corrosion potentials of X70 steel in NS4 solution are equal for specimens: from sheet -0.697 V, new pipe -0.681 V, pipe after 40 years of operation -0.689 V. The corresponding anodic slopes are 0.063, 0.038 and 0.036 V. The values of the steel corrosion rate are close, 0.053, 0.064 and 0.056 mm/year, which, according to the corrosion resistance scale, characterizes the steel in the NS4 solution as "resistant".

Stress-corrosion cracking of X70 steel specimens at potentials negatively the maximum protective potential -1.050 V occurs by the hydrogen embrittlement mechanism for a new pipe and for the sheet, and for pipe after 40 years of operation at this potential, stress-corrosion cracking is still possible by a mixed mechanism with a small contribution of anodic dissolution. At potentials more positive than minimum protective potential -0.750 V, by the anodic dissolution mechanism, stress-corrosion cracking occurs only for the steel sheet and pipe after 40 years of operation, and for the new pipe at the minimum protective potential, stress-corrosion cracking is possible by a mixed mechanism.

Some narrowing of the range of action of the mixed mechanism for a pipe after 40 years of operation compared to a new pipe, 0.368 and 0.160 V in the NS4 solution was noted. It was assumed that the differences are due to both changes in the metal during the manufacture of pipes on the one hand and the influence of operational factors.

- 6. Analyzing the features of corrosion-mechanical destruction of specimens at potentials from -0.750 V to -1.20 V, it was established that when the polarization potentials are shifted in the row -0.750 V  $\rightarrow$  -0.950 V  $\rightarrow$  -1.050 V  $\rightarrow$  -1.200 V, the susceptibility to stress-corrosion cracking in NS4, which is estimated by the coefficient Ks, changes for a steel sheet  $1.03 \rightarrow 1.09 \rightarrow 1.15 \rightarrow 1.40$ ; for a new pipe  $1.02 \rightarrow 1.10 \rightarrow 1.00 \rightarrow 1.00$ ; for a pipe after 40 years of operation  $-1.25 \rightarrow 1.34 \rightarrow 1.53 \rightarrow 1.86$ .
- 7. The following features of hydrogen penetration for the studied specimens were noted:
- for the sheet, maximum hydrogenation at a potential of -1.050 V (0.045 mole/dm $^3$ ), when potential shifted to -1.20 V the hydrogen concentration decreases to 0.018 mole/dm $^3$ ;
- for a new pipe and a pipe after 40 years of operation a gradual increase in hydrogenation when potential shifted from -0.950 to -1.200 V; for a new pipe, the amount of hydrogen increases from 0.0175 to 0.0296 mole/dm³ when potential shifted from -0.950 V to -1.050 V and stops at a value of 0.0301 mole/dm³ at a potential of -1.200 V. For samples from a pipe after 40 years of operation, the amount of hydrogen gradually increases from 0.0191  $\rightarrow$  0.0241  $\rightarrow$  0.0397 mole/dm³ with a potential shift of -0.950 V  $\rightarrow$  -1.050 V  $\rightarrow$  -1.200 V.

#### **ACKNOWLEDGMENT**

This research was carried out with financial support of the National Academy of Sciences of Ukraine (0122U001188).

#### **REFERENCES**

- [1] Živanović, Z., Petković, S., Mišanović, S., Holo, A., Šakota, Ž.: Natural gas buses in Serbia public transport: Some operational experiences, FME Transactions, 2015, Vol. 43, No.2, 89-98.
- [2] Sousa, S., Nunes, E., Lopes, I. Measuring and managing operational risk in industrial processes, FME Transactions, 2015, Vol. 43, No. 4, pp. 295-302.
- [3] Nykyforchyn, H., Krechkovska, H., Student, O., Zvirko O.: Feature of stress corrosion cracking of degraded gas pipeline steels, Procedia Structural Integrity, 2019, Vol. 16, pp. 153-160. https://doi.org/10.1016/j.prostr.2019.07.035
- [4] Zvirko, O.I., Kryzhanivskyi, E.I., Nykyforchyn, H.M., Krechkovska, H.V.: Methods for the Evaluation of Corrosion-Hydrogen Degradation of Steels of Oil-and-Gas Pipelines, Materials Science, 2021, Vol. 56, pp. 585–592. https://doi.org/10.1007/ s11003-021-00468-8
- [5] Nyrkova, L., Osadchuk, S., Goncharenko, L., Rybakov, A., Kharchenko, Y. O.: Influence of long -term operation on the properties of main gas pipeline steels. A review, Physics and Chemistry of Solid State, 2024, Vol. 25, No. 1, pp. 191–202. https://doi.org/10.15330/pcss.25.1.191-202
- [6] Nykyforchyn, H., Zvirko, O., Tsyrulnyk, O., Kret, N.: Analysis and mechanical properties characterization of operated gas main elbow with hydrogen assisted large-scale delamination, Engineering Failure Analysis, 2016, Vol. 82, pp. 364-377. https://doi.org/10.1016/j.engfailanal.2017.07.015
- [7] Nykyforchyn, H. M., Tsyrul'nyk, O.T., Petryna, D. Y., Hredil, M.I.: Degradation of steels used in gas main pipelines during their 40-year operation, Strength of Materials, 2009, Vol. 41, Is. 5, pp. 501–505.
- [8] Krechkovs'ka, H.V., Tsyrul'nyk, O.T., Student, O.Z.: In-Service Degradation of Mechanical Characteristics of Pipe Steels in Gas Mains, Strength Mater, 2019, Vol. 51, pp. 406–417. https://doi.org/10.1007/s11223-019-00087-4
- [9] Kryzhanivs'kyi, E.I., Nykyforchyn, H.M.: Specific features of hydrogen-induced corrosion degradation of steels of gas and oil pipelines and oil storage reservoirs, Mater Sci, 2011, Vol. 47, pp. 127–136. https://doi.org/10.1007/s11003-011-9390-9
- [10] Rybakov, A.A., Goncharenko, L.V., Filipchuk, T.N., Lokhman, I.V., Burak, I.Z.: Reasons of stress corrosion failure of girth joint of main gas pipeline, The Paton Welding Journal, 2014, Vol. 49, No. 3, pp. 49-52. https://doi.org/10.15407/tpwj2014.03.09
- [11] Nykyforchyn, H., In-service degradation of pipeline steels, in: Degradation Assessment and Failure

- Prevention of Pipeline Systems: ed. H. Nykyforchyn, G. Bolzon, G. Gabetta, H. Nykyforchyn (Springer, Cham.), 102, 15 (2020); https://link.springer.com/chapter/10.1007/978-3-030-58073-5 2.
- [12] Paton, B. E., Semenov, S. E., Rybakov, A. A., Vasilenko, S. K., Vasilyuk, V. M. The Paton welding journal, 7 (2000): p. 2-20 Paton, B. E., Semenov, S. E., Rybakov, A. A., Vasilenko, S. K., and Vasilyuk, V. M.: Ageing and procedure of evaluation of the state of metal of the main pipelines in service. Paton Welding Journal C/C of Avtomaticheskaia Svarka, 2000, No. 7, pp. 2-10.
- [13] Nyrkova, L. I., Goncharenko, L. V., Rybakov, A. O., Osadchuk, S. O., Klymenko, A. V., Kharchenko, Y. O.: Investigation of Welded Joints of Long-Term Operated Gas Pipeline Controllable Rolled X70 Steel, FME Transactions, 2023, Vol. 51, No. 1, pp. 71-80. https://doi.org/10.5937/fme2301071N
- [14] Polyakov, S.G., Rybakov, A.A.: The main mechanisms of stress corrosion cracking in natural gas trunk lines, Strength Mater, 2009, Vol. 41, pp. 456–463. https://doi.org/10.1007/s11223-009-9164-x
- [15] Nyrkova, L., Rybakov, A., Goncharenko, L., Osadchuk, S., & Kharchenko, Y.: Analysis of the causes of fracture of the main gas pipeline, Zastita Materijala, 2023, Vol. 64, No. 2, pp. 177-189. https://doi.org/10.5937/zasmat2302177N
- [16] Parkins, R. N.: Current Topics in Corrosion: Factors Influencing Stress Corrosion Crack Growth Kinetics, Corrosion, 1987, Vol. 43, No. 3, pp. 130– 139. https://doi.org/10.5006/1.3583125
- [17] Charles, E. A., Parkins, R. N.: Generation of stress-corrosion cracking environments at pipeline surfaces. Corrosion, 1995, Vol. 51, No. 7, pp. 518–527. https://doi.org/10.5006/1.3294372
- [18] Javidi, M., and Horeh, S. B.: Investigating the mechanism of stress corrosion cracking in nearneutral and high pH environments for API 5L X52 steel, Corrosion science, 2014, Vol. 80, pp. 213-220. https://doi.org/10.1016/j.corsci.2013.11.031
- [19] Shahriari, A., Shahrabi, T., and Oskuie, A. A.: A study on stress corrosion cracking of X70 pipeline steel in carbonate solution by EIS, Journal of materials engineering and performance, 2013, Vol. 22, pp. 1459-1470. https://doi.org/10.1007/s11665-012-0418-6
- [20] Fang, B. Y., Atrens, A., Wang, J. Q., Han, E. H., Zhu, Z. Y., and Ke, W.: Review of stress corrosion cracking of pipeline steels in "low" and "high" pH solutions, Journal of materials science, 2003, Vol. 38, pp. 127-132. https://doi.org/10.1023/A:1021126202539
- [21] Tang, X., and Cheng, Y. F.: Micro-electrochemical characterization of the effect of applied stress on local anodic dissolution behavior of pipeline steel under near-neutral pH condition, Electrochimica Acta, 2009, Vol. 54, No. 5, pp. 1499-1505. https://doi.org/10.1016/j.electacta.2008.09.037

- [22] Nyrkova L., Melnichuk S., Osadchuk S., Prokopchuk S., and Lisovyi P.: Investigating of the Mechanism of Stress Corrosion Cracking of Controllable Rolling Pipe Steel X70 In Near-Neutral Environment. Materials Proceedings, 2022. Vol. 50, Part 4, pp. 470-476. https://doi.org/10.1016/j.matpr.2021.11.294
- [23] Nyrkova, L. I., Klymenko, A. V., Osadchuk, S. O., and Kovalenko, S. Y .: Comparative investigation of electrolytic hydrogenation of pipe assortment steel under cathodic polarization, International Journal of Hydrogen Energy, 2024, Vol. 49, pp. 1075-1087. https://doi.org/10.1016/j.ijhydene.2023.06.316
- [24] Nyrkova, L. I., Klymenko, A. V., Goncharenko, L. Influence of electrolytic hydrogenation on stresscorrosion cracking of X70 steel and pipes of longterm exploited main gas pipeline, Journal of Hydrocarbon Power Engineering, 2023, Vol. 10, No. 1, pp. 15-24. https://doi.org/10.31471/2311-1399-2023-1(19)-15-24
- [25] de Sena R. Antunes, Bastos I. Napoleão, Plat G. Mendes: Theoretical and Experimental Aspects of the Corrosivity of Simulated Soil Solutions, International Scholarly Research Notices, 2012, Article ID 103715, 6 pages. https://downloads. hindawi.com/archive/2012/103715.pdf.
- [26] Nyrkova, L.: Stress-corrosion cracking of pipe steel under complex influence of factors, Engineering Failure Analysis, 2020, Vol. 116, 104757. https://doi.org/10.1016/j.engfailanal.2020.104757
- [27] ISO 17081:2014. Method of measurement of hydrogen permeation and determination of hydrogen uptake and transport in metals by an electrochemical technique
- [28] State standard of Ukraine ISO 643:2009 (ISO 643: 2003, IDT) Steels. Micrographic method determination of the apparent grain size.
- [29] State Standard of Ukraine 8974:2019 Steel. Metallographic method for evaluating the microstructure of sheets and strips.
- [30] ISO 3183:2019 Petroleum and natural gas industries — Steel pipe for pipeline transportation systems.
- [31] TR 14-3-995-81. Steel pipes straight-seam expanded with a diameter of 1420 mm made of X70 steel.
- [32] State standard of Ukraine 4219:2003 Steel pipe mains. General requirements for corrosion protec—tion

#### **NOMENCLATURE**

$b_a$	Tafel slope of the anodic polarization curve
$C_{H_2}$	concentration of hydrogen penetrating through

hydrogen diffusion coefficient  $D_{H_2}$ 

 $D^{ef}$ effective coefficient of diffusion of hydrogen  $H_2$ 

Е potential

null current potential of the slow rate  $E_0^1$ (0.5 mV/s) polarization curve

- null current potential of the fast rate  $E_0^2$ 
  - (100 mV/s) polarization curve
- $E_{cor}$ corrosion potential
- $E_{pol}$ polarization potential É Faraday constant
- Ι current strength
- i current density
- background current  $I_b$
- current caused by hydrogen penetration  $I_{H_{,}}$
- current in the stationary regime of hydrogen  $I_{st}$ 
  - penetration
- stress-corrosion cracking susceptibility  $K_S$
- coefficient
- specimen's square or cross-sectional area of a S
- specimen
- cross-section area of specimens before tests  $S_0$
- cross-section area of specimens in the place of  $S_1^{sol}$
- fracture after tests
- corrosion rate  $v_{cor}$

#### Greek symbols

- δ relative
- 3 elongation
- stress
- yield stress  $\sigma_{v}$
- tensile strength  $\sigma_{st}$
- time duration
- relative narrowing

#### Superscripts and subscripts

- anodic a
- h background
- corrosion cor
- ef effective
- $H_2$ hydrogen
- solution sol ts tensile stress
- yield

#### АНАЛИЗА УТИЦАЈА ДУГОТРАЈНОГ РАДА ГАСОВОДА ОД ЧЕЛИКА Х70 НА ПОДЛОЖНОСТ ПУЦАЊУ ПОД НАПОНСКОМ КОРОЗИЈОМ У РАСТВОРУ СКОРО НЕУТРАЛНОГ РН ПОД КАТОДНОМ ПОЛАРИЗАЦИЈОМ

#### Л. Ниркова, Л. Гончаренко, С. Осадчук, Ј. Харченко

Пуцање под напонском корозијом основног метала линеарног дела главног гасовода од челика X70 након рада током 40 година у раствору скоро неутралног pH NS4 испитивано је у поређењу са цеви која није била у употреби и челичним лимом. Затезна чврстоћа и граница течења свих проучаваних узорака испуњавају захтеве стандарда ISO 3183, али је релативно издужење узорака из цеви нешто испод нормализоване вредности. Потенцијали корозије су слични и једнаки су -0,697 V за челични лим, -0,681 V за нову цев, -0,689 за експлоатисану цев, а брзине корозије су 0,053, 0,064 и 0,056 mm/годишње, респективно, што одговара групи отпорности "стабилно". Пуцање услед напонске корозије при потенцијалима негативнијим од максималног заштитног -1,050 V настаје механизмом водоника за нову цев, а за лим и цев након 40

година рада - механизмом анодног раст-варања и водоничне кртости са малим доприносом анодног растварања. При потенцијалу од -1,050 V, продор водоника је највећи за челични лим (0,045 mol/dm3), за нову цев и цев након 40 година рада - вредности су сличне, 0,0296 и 0,0241 mol/dm3, респективно.